Morphology of Direct SLS-Processed Stainless Steel Layers

Mr. C. Martin Taylor, Prof. T.H.C. Childs, Mr. C. Hauser

School of Mechanical Engineering, University of Leeds, Leeds LS2 9JT, UK

Email: mencmt@leeds.ac.uk;   Tel. : +44 (0)113 233 2143

ABSTRACT

This paper discusses work done to analyse the shape of stainless steel layers generated by direct selective laser sintering (SLS). Laser power, scan spacing and scanning speed have been varied, to investigate their effect on geometry. The relationship between scanning parameters and the qualities of sintered parts (dimensional uniformity, porosity and scanned track shape) is described. A PC-based finite element code, developed to simulate SLS, has been modified to match the conditions of experiments discussed above. A comparison is made between computer-generated and experimentally-generated parts.

Keywords: Direct laser sintering, stainless steel powder, modelling, visualisation, dimensions

1. INTRODUCTION

1.1 Background

In developing a solid freeform fabrication (SFF) process, it is desirable that parts are manufactured in as short a time as possible, utilising a minimum number of stages. One such process, selective laser sintering or SLS, has become popular for rapidly manufacturing freeform parts using a wide range of materials [1]. Moulding tools and other metallic parts are made relatively quickly by SLS coupled with post processes. Other SFF methods are under development in which metallic freeform parts are fabricated directly with a scanning laser beam [2, 3]. Laser-based freeform fabrication of metals shows great promise, but more progress is required. Levels of dimensional accuracy, surface finish and mechanical properties aimed for are those displayed by metal forming processes such as machining.

The hardware discussed in this paper is designed for the direct laser processing of metallic parts, from a room temperature powder bed. In order to improve the quality of parts produced in this way, phenomena associated with the process and the material to be processed must be understood. Experimental and computer-based modelling studies have been undertaken for this purpose. Single lines and layers of stainless steel material have been manufactured with a variety of laser parameters and scanning procedures in order to minimise curling and cracking [3]. Meanwhile, a finite element (FE) transient-state thermal model has been written and developed in Fortran to simulate the SLS process, being the subject of previous papers. Several variants of the model exist: for amorphous polymers, crystalline polymers [4, 5] and most recently a 3-dimensional (3D) version for metals [5].

To support modelling activity, a range of experiments have been conducted to find material properties [4, 5, 6] and to compare model output with in-process and post-process measurements. A stress model of deformation due to heat-induced expansion and shrinkage in SLS has been developed separately [7].

530

The magnitude of temperature variation with position and time in the direct metal SLS process described is relatively large. Steel is converted from powder into a solid structure, experiencing peak temperatures some way beyond its melting point. In this sense, the heat transfer and material flow encountered in the process may be more akin to that found in laser welding [8, 9] than in traditional sintering.

1.2 Experimental Manufacturing Work

Experiments were undertaken to produce 27 single layer parts from stainless steel powder using bespoke layered manufacturing equipment. Geometrical characteristics of each part were analysed. The form of parts was related to the processing conditions used. Special attention was given to any unusual effects which have not yet been accounted for.

Geometrical analysis took place on part cross-sections, because sectional analysis is currently easier than volumetric analysis. Parameters changed in experiments were:
laser power P;   laser scanning speed U;   scan spacing s.

1.3 Modelling Work

The Fortran sintering model was run with the same process parameter values used for manufacturing real parts. The manufactured layers were compared dimensionally to post-processed model output. New post-processing tools have been developed which can make more use of output, improving quality of feedback and reducing the amount of effort required in repetitive tasks. So as well as verifying the model against experiment, it was attempted to improve the verification process.

2. DESCRIPTION OF EQUIPMENT AND MODEL
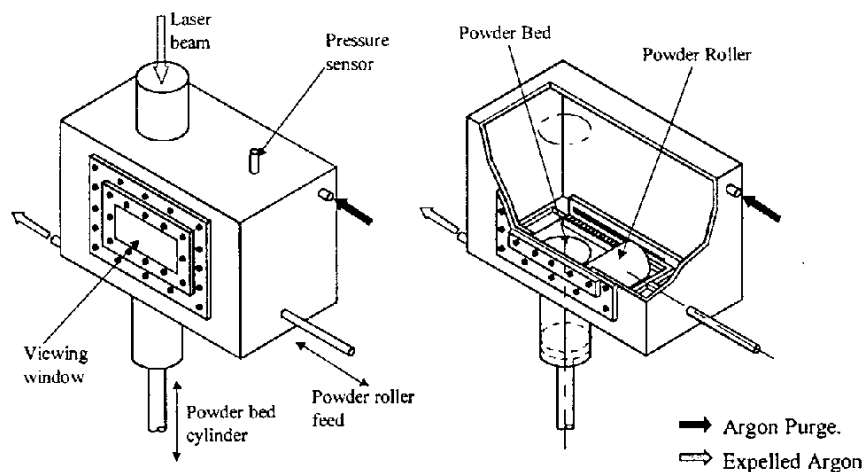
2.1 Direct High-Temperature Sintering Rig

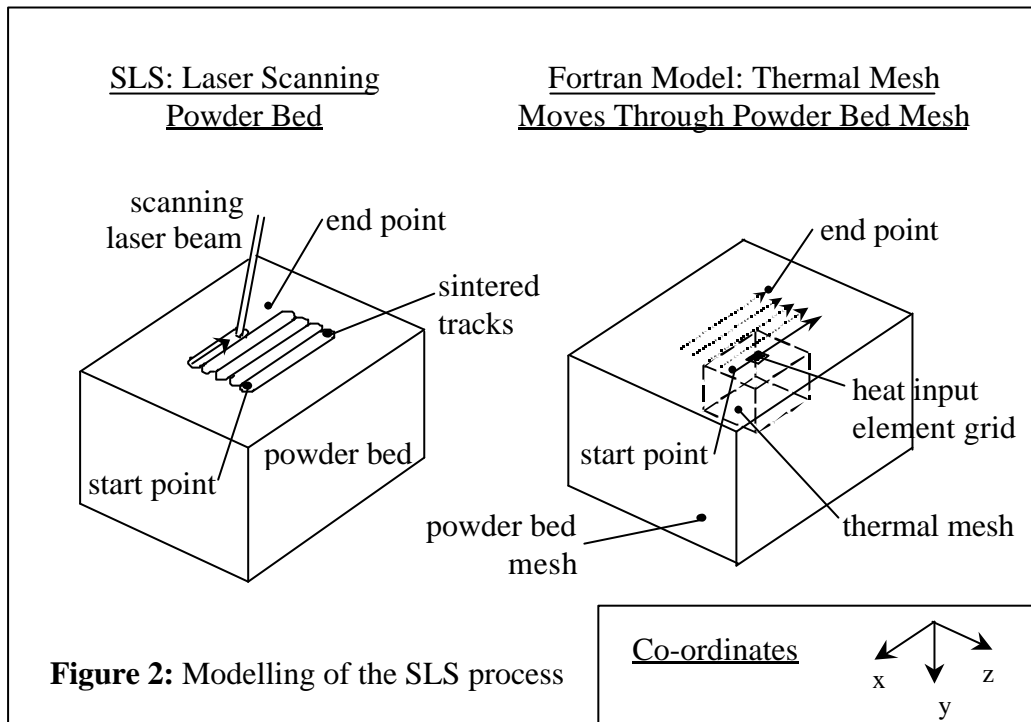**Figure 1**: Experimental apparatus

Experiments were carried out in a vacuum chamber (Figure 1). A window in the chamber's ceiling allowed the laser beam to enter. A detachable viewing window allowed observation of the process, and access between experiments. A pump and argon bottle were attached to the chamber so that the air inside could be replaced with an inert atmosphere for sintering. No powder preheating was provided.

The processing laser was of 250W CW carbon dioxide type, wavelength 10.6μm, beam diameter 1.1mm. The laser sintered the material directly. The material used was gas-atomised stainless steel 314S powder, size distribution 75-150μm and composition as in Table 1.

Element	Fe	Ni	Cr	C	Si	P	Mn	S
Percent	Bal.	19.85	24.36	0.443	1.43	0.017	0.94	0.006

Table 1: Stainless Steel 314S Powder Composition

2.2 Fortran Finite Element Model

Figure 2: Modelling of the SLS process

The model developed is of transient-state thermal type, with calculations carried out in 3 dimensions using tetrahedral-shaped quadrilateral volume elements. Figure 2 illustrates the modelling concept. Two meshes are utilised, a powder bed mesh (PBM) and a smaller thermal mesh (TM). The PBM stores density, temperature and other information for nodes throughout the powder bed. The TM contains heat transfer elements, including a grid for heat input (Fig. 2). Heat input intensity follows a discretised Gaussian distribution across the grid surface, and reduces exponentially over a finite depth. The TM marches through the PBM in a predefined pattern (Fig. 2), operating on the PBM values falling within its volume.

At each step in the program a repeated sequence of events occurs. The TM advances by one PBM element length, then reads PBM data. A FE calculation follows, where temperatures are calculated through the governing equation (which is conduction-based in the body of the TM). Specific heat and conductivity of each node are recalculated based on temperature and density. If the temperature at a node falls within the latent phase of steel where solid and liquid both exist, solid fraction is calculated based on temperature (using a temperature recovery method) then density is calculated based on solid fraction. Shrinkage of the powder bed in the depth direction due to density change is included.

Heat steps occur sequentially until all scans and layers are complete. The powder bed holds the final values for nodes processed by the thermal mesh. This data is written to a text file, with one line of characters per node. Each line contains the nodal x, y and z co-ordinates, then the corresponding material density *Rho*. No account is made of thermal expansion or surface tension effects in the model, and there are no stress calculations.

3. EXPERIMENTS AND MODELLING ACTIVITY

3.1 Manufacture of Steel Layers

The equipment described in Section 2.1 was used to create single layers from the stainless steel powder. Before sintering, an inert atmosphere was created. The chamber pressure was reduced to 40mbar then the chamber was back-filled with argon gas. This expulsion and back-fill was carried out twice, before a 10 minute purge of argon with positive internal pressure. Argon continued to flow through the chamber during sintering.

Each part was a single layer, made of 10 uniformly- spaced parallel scans of the laser beam. All scans were 10mm long. Scanning was unidirectional, although this is considered arbitrary at present: both the equipment and the model are capable of raster scanning. 3 parts were made at each of 9 scanning conditions. The scanning conditions were as shown in Table 2, where d is the laser beam diameter (1.1mm). The parameter values have been chosen from within a range reported as leading to manufacture of high quality single tracks [3].

	P=60W, U=1mm/s	P=120W, U=6mm/s	P=155W, U=12mm/s
$s = 3\,d\,/6$	3 parts	3 parts	3 parts
$s = 5\,d\,/6$	3 parts	3 parts	3 parts
$s = 9\,d\,/6$	3 parts	3 parts	3 parts

Table 2: Experimental sintering machine parameters

3.2 Scan Surface Shape Change Study: Manufacture of Single Scans

Manufacturing single scans at high values of P and low U, a point was reached where the power/ speed combination led to a conspicuous change in scan cross-sectional shape. Decreasing U past this point, an increase in energy delivered (P/U) was causing the mass of material melted to reduce. This is the reverse of what is expected. A brief investigation into this phenomenon has been carried out. Sets of 5 separate steel scans were made at two P and U combinations, either side of the observed transition point. These were:
Experiment **A**: P= 160W, U= 0.5mm/s   Experiment **B**: P= 160W, U= 1.0mm/s.
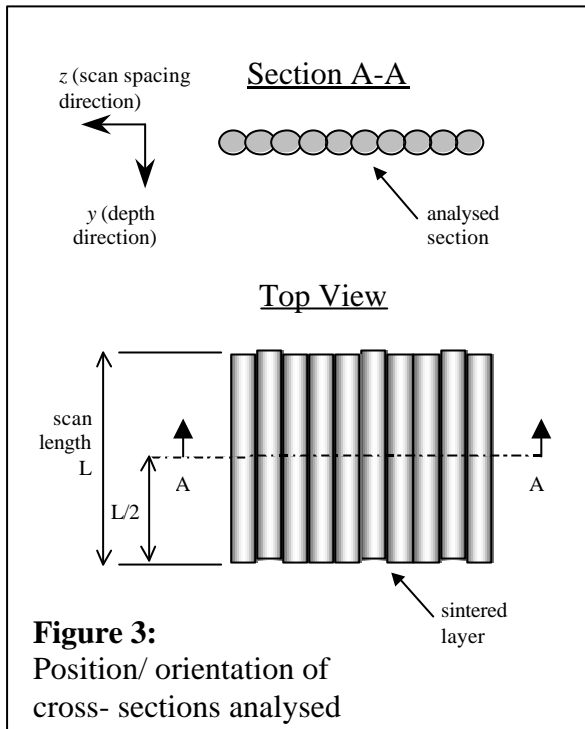
3.3 Modelling of Steel Layer Manufacture

The Fortran model developed for steel was run 9 times, using the same input values for s, P and U as in the manufacturing experiments. Output files as described in Section 2.2 were generated, ready for post-process manipulation.

4. PROCESSING OF RESULTS

4.1 Preparation and Analysis of Steel Cross-Sections

Once made, each layer was set in protective epoxy resin, then sectioned as shown in Figure 3. This revealed the cross-section of the layer down it's centre in the scan direction. A

Figure 3:
Position/ orientation of
cross- sections analysed

profilometer and digital camera were used to convert cross-sections into computer images which were analysed dimensionally. Analysis was semi-automated, using Image-Pro Plus software (V3, Media Cybernetics L.P.). Image-Pro can calculate the size of a discrete area, given an image calibration value.

Image-Pro was used to evaluate the cross-sectional solid area of the manufactured samples. It was also able to automatically generate a convex hull round the exterior of sections, in order to evaluate their percentage of full density.

4.2 Post-Processing of Model Output

The co-ordinate and density data generated has been post-processed in two ways. Firstly, Matlab V6 (The MathWorks Inc.) analysed density in 3D to create a surface joining points of equal value, like contour lines on a map. Lighting and viewing angle on the "modelled part" generated can be changed as with a CAD model. Secondly, GSharp V3.1 (AVS Inc.) was used to produce 2D sectional views of modelled parts, with the option of a superimposed grid for manual dimensional analysis. Image-Pro was used on GSharp-generated 2D mid-scan sections as described in Section 4.1, to evaluate cross-sectional area and relative density.

5. RESULTS

Figures 4 and 5 show, as an example, a manufactured single layer and a modelled single layer respectively. In both cases the layer is made at $s= 5d/6$, $P= 60W$, $U= 1mm/s$. The accompanying scales are graduated in millimetres. Figure 6 shows mid-scan sections of the Figure 4 and 5 layers.

Table 3 displays sectioned layers processed with variables as stated in Table 2. The calculated cross-sectional area and relative density of manufactured and modelled parts is reported for comparison. In both Figure 6 and Table 3, the first line scanned is always on the left-hand end of the section.

Results from the scan surface shape change study (Section 3.2) are shown in Figure 7.
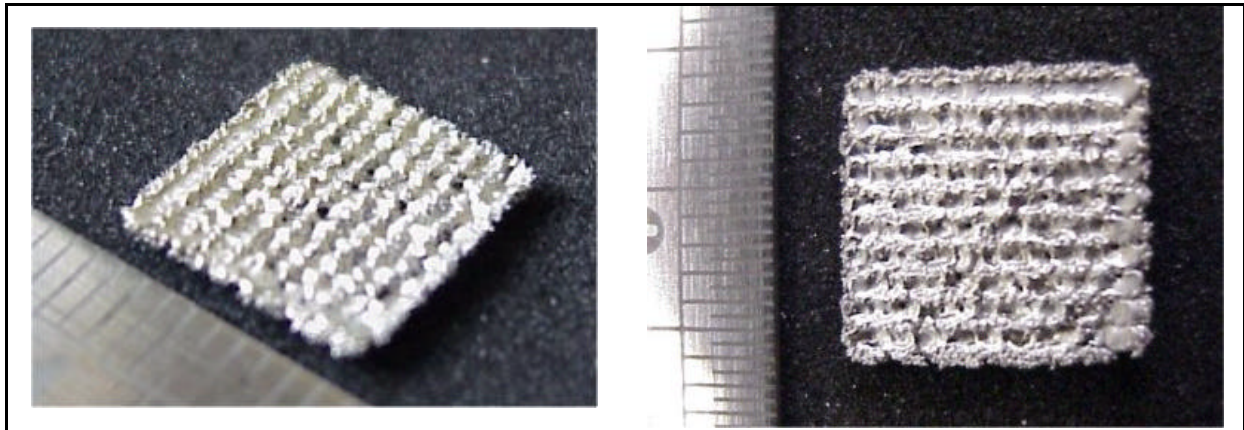
Figure 4: Perspective (above left) and top view (above right) of example manufactured part
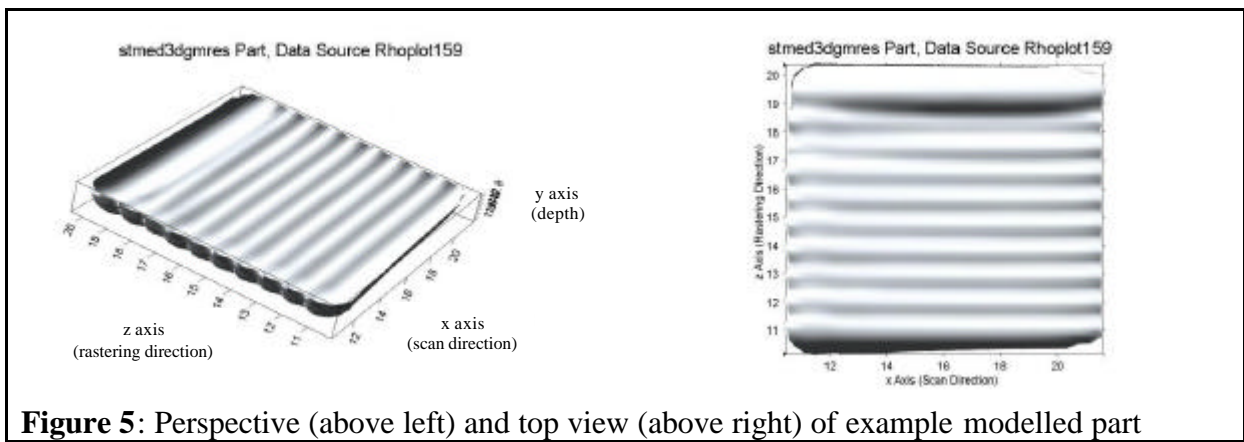

Figure 5: Perspective (above left) and top view (above right) of example modelled part

Figure 6: Mid-scan sectional views of the same manufactured (left) and modelled (right) part

Conditions		Manufactured Parts			Modelled Parts		
s (mm) [d= 1.1 mm]	P (W), U (mm/s)	Example Profile	Solid Area (mm^2)	Rel've Density (%)	Profile	Solid Area (mm^2)	Rel've Density (%)
3d/6	60, 1		5.0	68		3.4	76
	120, 6		4.2	63		3.2	72
	155, 12		3.8	66		2.9	78
5d/6	60, 1		6.7	59		5.0	73
	120, 6		6.4	64		4.8	76
	155, 12		7.1	65		4.1	78
9d/6	60, 1		10.5	58		7.3	57
	120, 6		12.2	56		7.1	64
	155, 12		8.8	45		5.8	58

Table 3 Comparison of modelled and manufactured part cross-sections

Figure 7: Two 10mm scans

One scan processed at 160W, 0.5 mm/s (left), other processed at 160W, 1.0 mm/s (right).

Energy delivered to left hand scan = 3200 J.
Mass of scan = 0.52 g.

Energy delivered to right hand scan = 1600 J.
Mass of scan = 0.73 g.

6. DISCUSSION

6.1 Morphology of Manufactured and Modelled Parts

With reference to Table 3, the geometrical features of layers will be considered, and a comparison will be made between manufactured and modelled parts. Despite some 2D cross-sections displaying areas isolated by pores, all parts manufactured for this study are coherent.

At 1mm/s scan speed, a flattened track surface profile is seen in manufactured parts. This relates to the phenomenon to be discussed in Section 6.2. At U of 6 and 12mm/s track surfaces are rounded in the molten state, by surface tension at low viscosity. The rounding of track surfaces is not predicted by the model.

Low s, high P and low U lead to high energy input per unit area of the powder bed. For this reason, parts made at parameters 3d/6-60-1 are expected to have a higher sintered density than parts processed at 9d/6-155-12. The relationship between energy per unit area and relative density is not a linear one however, as can be deduced from Table 3.

Experiments and modelling agree that the amount of material melted decreases with decreasing s. Previously-processed material can act as a heat sink for laser energy, and this effect increases with reduction of s. Furthermore, rescanned solid metal absorbs a lower proportion of incident laser energy than fresh powder [6]. The heat sink effect is recreated in modelling, but the absorption effect is not. These two effects mean that the first (left-hand in Table 3) laser scan melts more material than following scans for the majority of manufactured layers. The first scan is always the largest in modelled parts. Sectional area size comparison shows that the model underestimates the amount of material melted experimentally: this may be because powder bed mesh temperatures are reset to ambient level before each new scan. The amount of heat discarded through this practice will be analysed in future work.

Experimentally-generated parts display a lower relative density than modelled ones. In general, the shape of real parts is more irregular and jagged. Lowest relative density occurring at s= 9d/6 is correctly predicted by the model. Higher roughness is observed at high scan spacing in both manufactured and modelled parts; the curvature of individual scans is more distinct. Variation is seen in batches of identically-processed manufactured parts, whilst modelled parts do not change shape when a simulation is repeated.

6.2 Scan Surface Shape Change Study

When weighed, scans processed at 160W and 1.0mm/s had on average 40% more mass than those created at 0.5mm/s. This is despite their only receiving half the incident laser

energy by comparison. Some phenomenon is causing a reduction in the proportion of laser energy usefully melting the steel. It is observed in Figure 7 that the surface of the lighter scan is depressed, not an effect likely to be caused by surface tension. The reduction in absorbed energy and concave surface resemble the effects of metal vapour plasmas, seen in laser welding [9]. Therefore it is suggested that at certain high values of P (greater than 50W) and low U (below 3mm/s), steel is being caused to vaporise, the resulting recoil pressure depressing the scan surface. Accounting for vaporisation and plasma generation adds complexity to the modelling process; however, for the majority of power and speed values considered the phenomenon is not observed.

6.3 Development of Tools to Support Modelling

Use of Image-Pro software has eased the task of sectional area analysis. 3D views generated using Matlab are convenient for rapid verification of parts, and for communication of output. The programming power of Matlab means that scripts could be written to evaluate properties such as surface roughness, volume and mass of modelled parts in the future.

7. CONCLUSIONS

Metal layers processed by direct SLS have been compared in shape to the output from a numerical model of the process. The model correctly predicts trends in the amount of material melted and relative density related to process parameters. New post-processing tools developed can ease model refinement. A shape change phenomenon is seen in real parts made at high laser energy density, this is believed to be caused by metal vaporisation.

8. REFERENCES

1. Pham, D.T., Gault, R.S. (1997): "A Comparison of Rapid Prototyping Technologies", *International Journal of Machine Tools and Manufacture*, No.38, pp.1257-1287
2. O'Neill, W. (1998): "Investigation of Short Pulse Nd:YAG Laser Interaction with Stainless Steel Powder Beds", *Proceedings of the Solid Freeform Fabrication Symposium 1998*, University of Texas, Austin, Texas, USA, pp.147-153
3. Hauser, C., Childs, T.H.C., Dalgarno, K.W. (1999): Selective Laser Sintering of Stainless Steel 314S HC Processed Using Room Temperature Powder Beds", *Proceedings of the SFF Symposium 1999*, pp.273-280
4. Childs, T.H.C., Tontowi, A.E. (2001): "Selective Laser Sintering of a Crystalline and a Glass-Filled Crystalline Polymer: Experiments and Simulations", *Proceedings of the Institution of Mechanical Engineers*, Vol. 215, Part B, pp.1481-1495
5. Childs, T.H.C., Hauser, C., Tontowi, A.E., Taylor, C. (2000): "Simulation and Experimental Verification of Crystalline Polymer and Direct Metal Selective Laser Sintering", *Proceedings of the SFF Symposium 2000*, pp.100-109
6. Taylor, C.M., Childs, T.H.C.C. (2001): "Thermal Experiments in Direct Metal Laser Sintering", *Proceedings of Euro RP 2001*, Process Development Session
7. Dalgarno, K.W., Jamal, N. (2002): "Analysis of the Influence of Viscoelasticity in Curl Development in SLS", *Proceedings of this Conference*
8. Dowden, J., Davis, M., Kapadia, P. (1981): "Some Aspects of the Fluid Dynamics of Laser Welding", *Journal of Fluid Mechanics*, Vol.126, 1983, pp.123-146
9. Equilasers, Inc. (2001): "Laser Micro-Welding for the Photonics Industry", *Business Briefing.* Source: www.wmrc.com